CHEMISTRY OF MATERIALS

Subscriber access provided by - Access paid by the | UCSB Libraries

Article

Towards Stable Deep-Blue Luminescent Colloidal Lead Halide Perovskite Nanoplatelets: Systematic Photostability Investigation

Seung Kyun Ha, Catherine M. Mauck, and William A. Tisdale

Chem. Mater., **Just Accepted Manuscript** • Publication Date (Web): 18 Mar 2019

Downloaded from http://pubs.acs.org on March 18, 2019

Just Accepted

"Just Accepted" manuscripts have been peer-reviewed and accepted for publication. They are posted online prior to technical editing, formatting for publication and author proofing. The American Chemical Society provides "Just Accepted" as a service to the research community to expedite the dissemination of scientific material as soon as possible after acceptance. "Just Accepted" manuscripts appear in full in PDF format accompanied by an HTML abstract. "Just Accepted" manuscripts have been fully peer reviewed, but should not be considered the official version of record. They are citable by the Digital Object Identifier (DOI®). "Just Accepted" is an optional service offered to authors. Therefore, the "Just Accepted" Web site may not include all articles that will be published in the journal. After a manuscript is technically edited and formatted, it will be removed from the "Just Accepted" Web site and published as an ASAP article. Note that technical editing may introduce minor changes to the manuscript text and/or graphics which could affect content, and all legal disclaimers and ethical guidelines that apply to the journal pertain. ACS cannot be held responsible for errors or consequences arising from the use of information contained in these "Just Accepted" manuscripts.

ACS Publications

is published by the American Chemical Society. 1155 Sixteenth Street N.W., Washington, DC 20036

Published by American Chemical Society. Copyright © American Chemical Society. However, no copyright claim is made to original U.S. Government works, or works produced by employees of any Commonwealth realm Crown government in the course of their duties.

Towards Stable Deep-Blue Luminescent Colloidal Lead Halide Perovskite Nanoplatelets: Systematic Photostability Investigation

Seung Kyun Ha,[†] Catherine M. Mauck,[†] William A. Tisdale*[,†]

[†]Department of Chemical Engineering, Massachusetts Institute of Technology, Cambridge, Massachusetts 02139, United States.

colloid, lead halide, perovskite, nanoplatelet, nanosheet, nanocrystal, 2D, Ruddlesden-Popper, quantum confinement, stability

ABSTRACT: Colloidal lead halide perovskite nanocrystals and nanoplatelets have emerged as promising semiconductor nanomaterials due to their spectral tunability, facile processability, and bright emission with high color purity. In particular, strong quantum- and dielectric confinement make atomically thin colloidal lead bromide perovskite nanoplatelets a favorable candidate for next-generation deep-blue-emitting (λ_{max} = 437 nm) materials. However, poor photostability poses a critical challenge; colloidal nanoplatelets suffer from photobleaching or transformation into thicker, less-confined nanostructures with red-shifted emission upon UV irradiation. In this study, we synthesize deep-blue-emitting organic-inorganic hybrid perovskite nanoplatelets (Formula: $L_2[ABX_3]BX_4$, L: butylammonium and octylammonium, A: methylammonium or formamidinium, B: lead, X: bromide or iodide) with large lateral dimension (~1 μm) by ligand-assisted reprecipitation and systematically investigate the factors that affect the photostability of those nanoplatelets. We find that freshness of the prepared precursor solutions for ligand-assisted reprecipitation is critical to obtain better stability with high photoluminescence quantum yield of perovskite nanoplatelets. Photobleaching is found to result from intrinsic instability of the perovskite lattice against UV irradiation in nanoplatelets, while transformation into thicker nanostructures results from extrinsic factors – moisture, primarily. Furthermore, we observe that substitution of the organic cation from formamidinium to methylammonium and addition of excess alkylammonium bromide ligands significantly enhances both the ambient and photostability. Lastly, we demonstrate that the dropcast film of methylammonium lead bromide nanoplatelets with excess alkylammonium bromide ligands shows dramatically improved stability both under UV irradiation and under ambient conditions. This study expands our understanding of the factors that affect perovskite nanoplatelet photostability and opens up new possibilities for the fabrication of stable perovskite-nanoplatelet-based optoelectronic devices.

Introduction

One of the most successful commercial applications of semiconductor nanomaterials is in light-emitting technologies.[1] However, achieving efficient deep-blue luminescence – required for a wide color gamut – has been challenging, compared to the state-of-the-art red and green luminescence. Blue-emitting devices fabricated with wide-bandgap semiconductor materials still suffer from limited operational lifetime, efficiency roll-off, low charge carrier mobility, relatively low efficiency compared to green and red analogues, and high manufacturing cost.[2-7]

Recently, lead halide perovskites, with formula ABX_3 (A = small cation, B = Pb, X = Cl, Br, I), have emerged as a promising class of materials for optoelectronic applications. Rapid development of perovskite solar cells[8-11] has demonstrated their fascinating properties such as low-temperature synthesis,[12] long charge carrier diffusion lengths,[13-16] wide compositional tunability[17-18] and defect tolerance.[19-20] Furthermore, when prepared as colloidal 3D nanocrystals,[21-24] lead halide perovskites can achieve large exciton binding energies on the order of hundreds of meV[25-26] and bright luminescence.[27-29] Deep-blue luminescence from ABX_3 perovskites has been attempted through chloride incorporation to shift the band gap to higher energies or by reducing the size of quantum dots,[30-33] yet efficient deep-blue luminescence has been elusive. Instead, two-dimensional (2D) lead bromide perovskites ($L_2[ABX_3]BX_4$, where L = butylammonium or octylammonium) have emerged for deep blue luminescent applications due to their strongly quantum- and dielectric-confined nature, leading to thickness-dependent tunability and spectrally narrow emission with small Stokes shifts.[34-44] Directional light emission, previously observed in other 2D semiconductor nanomaterials,[45-46] further highlights the possibility of enhancing the outcoupling efficiency of 2D-perovskite-based devices. Multiple methods have been reported on the synthesis of 2D perovskites including ligand-assisted reprecipitation,[34, 38, 44] hot-injection synthesis,[36, 40] and layered perovskite crystal growth.[41, 43, 47] Colloidal 2D perovskites, sometimes referred to as perovskite nanoplatelets, are highly promising for their additional property of solution processability. However, progress in blue light emission from 2D perovskites has lagged behind that of red- and green-emitting materials, and their optoelectronic devices either do not reach the deep-blue region,[48-51] are low in efficiency,[35, 52] or are unstable under operating conditions.[35, 52]

Many authors have noted that lead bromide perovskite nanoplatelets undergo significant changes to their optical properties when exposed to ultraviolet (UV) light.[34, 53] Poor photostability poses a crucial obstacle to realizing commercial light-emitting technologies, yet comprehensive understanding of the factors influencing photostability in perovskite nanoplatelets is lacking. In this work, we synthesize colloidal organic-inorganic hybrid lead bromide nanoplatelets, which emit in the deep-blue region (λ_{max} = 437 nm), by facile ligand-assisted reprecipitation methods. We then categorize the photoinstability of perovskite nanoplatelets into two aspects: photobleaching, which refers to the decrease in photoluminescence (PL) intensity, and transformation, resulting in the emergence of PL peaks with different wavelengths from the original peak. We find that using freshly prepared precursor solutions dramatically enhances the stability, in addition to substituting formamidinium for methylammonium and isolating samples from moisture. Lastly, we show that adding excess alkylammonium bromide surface capping ligands further enhances the intrinsic stability of nanoplatelets. Dropcast films of nanoplatelets with excess ligands exhibit impressive stability both under UV and under ambient conditions. These photostability studies on colloidal perovskite nanoplatelets serve as a guide for future fabrication of stable and efficient deep-blue emitting devices.

Experimental Methods

Colloidal perovskite nanoplatelet synthesis:

Colloidal perovskite nanoplatelets were synthesized using the ligand-assisted reprecipitation method under N_2 atmosphere in a glovebox. Individual precursor solutions were prepared by dissolving precursor salts (AX, BX_2, LX) in anhydrous N,N-dimethylformamide (DMF) at the concentration of 0.2M. Those precursor solutions were then mixed in specific ratio to achieve desired thickness and composition (See the Supporting Information file for details). A 1:1 mixture of butylammonium and octylammonium was used as the capping ligand. To form nanoplatelets, 10 µL of this mixed precursor solution (unless stated otherwise) was dropped into 10mL of toluene under vigorous stirring. To ensure complete crystallization, solutions were left under stirring for 5 minutes (for bromide nanoplatelets) or 10 minutes (for iodide nanoplatelets).

Photostability experiment:

Solution: 2.5 mL of as-synthesized colloidal perovskite nanoplatelet solutions were transferred into quartz cuvettes under specified atmospheric conditions and irradiated with continuous-wave UV light from a 365 nm fiber-coupled LED (Thorlabs) at specified intensity, while stirring, with photoluminescence spectra taken every 6 seconds. Absorption spectrum of the solution was measured before and after UV irradiation.

Film: For thin film studies, perovskite nanoplatelets were synthesized in larger quantity by dropping 100 µL of precursor solution into 10 mL toluene. Then, nanoplatelets were centrifuged at 4300 rpm for 10 minutes, redispersed in 100 µL toluene, drop-cast onto glass slides and dried under vacuum. Thin film samples were irradiated by continuous-wave UV light from a 365 nm fiber-coupled LED (Thorlabs) at the specified intensity, with photoluminescence spectra taken every 6 seconds.

Atmosphere control: A vacuum pump and N_2 feed were used to control the atmosphere inside Aldrich AtmosBag, with a water bath and the desiccant (MiniPax absorbent packets) controlling the relative humidity.

Characterization:

Photoluminescence spectra (PL): PL spectra were collected using an Avantes fiber-optic spectrometer. 365 nm fiber-coupled LED (Thorlabs) was used to excite samples.

Absorption spectra: Absorption spectra were taken using Cary 5000 UV-vis spectrophotometer.

Photoluminescence quantum yield (PLQY): PLQY measurements were performed using an integrating sphere and Avantes fiber-optic spectrometer.[54] 405 nm laser diode (Thorlabs) was used to excite samples.

Fourier transform infrared spectroscopy (FTIR): FTIR was performed using a Thermo Fisher 6700 FTIR spectrometer. FTIR samples were drop cast onto NaCl (Real Crystal IR samples cards, International Crystal Laboratories). Spectra were background subtracted, normalized and smoothed with 5-point adjacent averaging for comparison.

^{1}H nuclear magnetic resonance (NMR): NMR spectroscopy was performed on a Bruker AVANCE III – 400 NMR spectrometer. NMR samples were prepared by drying aged MABr-DMF solutions under N_2, then redissolving the residue in deuterated DMF. NMR spectra were normalized with respect to DMF CH peak intensity and analyzed in MNova (v. 12.0.0, Mestrelab Research.)

Transmission electron microscopy (TEM): TEM images were taken using FEI Tecnai G2 Spirit Twin instrument operating at 120kV. TEM samples were prepared by centrifuging nanoplatelets, redispersing in small amounts of toluene (~ 300 µL) and drop-casting onto TEM grids.

Scanning electron microscopy (SEM): SEM images were taken using Zeiss Merlin instrument operating at 5kV. SEM samples were prepared by making large quantity of nanoplatelets by dropping 100 µL of precursor solution into 10 mL toluene, centrifuging nanoplatelets, redispersing in 100 µL toluene and then drop-casting onto silicon wafer substrates.

X-ray diffraction (XRD): XRD was performed using a PANalytical X'Pert Pro operating at 45 kV and 40 mA with a copper radiation source. HighScore Plus software was used to subtract the background. XRD samples were prepared by making large quantity of nanoplatelets by dropping 100 µL of precursor solution into 10 mL toluene, centrifuging nanoplatelets, redispersing in 100 µL toluene and then drop-casting onto glass slides.

X-ray photoelectron spectroscopy (XPS): XPS was performed using a Physical Electronics Versaprobe II. Spectra were charge corrected to put principal C1s peak at 284.8 eV, smoothed and normalized. XPS samples were prepared by centrifuging nanoplatelets, redispersing in small amounts of toluene (~ 30 µL) and drop-casting onto glass slides.

Dynamic light scattering (DLS): DLS was performed using a Wyatt Mobius with a 532nm laser. Measurements averaged 5 acquisitions of 10 seconds each, and autocorrelation curves were fitted using Wyatt Dynamics V7 software.

Results and Discussion

Nanoplatelet Synthesis and Characterization

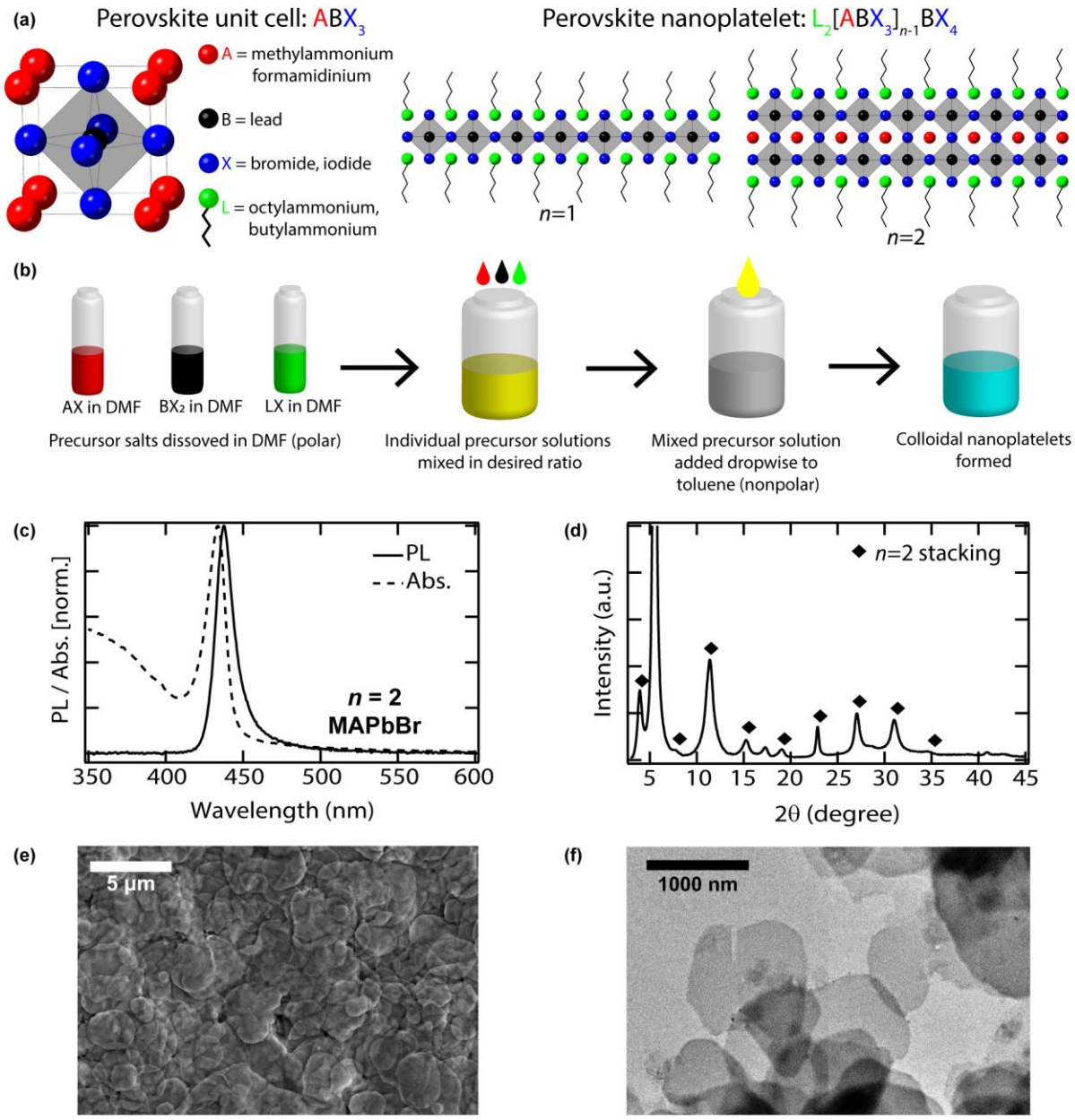

Figure 1. *Synthesis and characterization of lead halide perovskite nanoplatelets.* (a) Structures of perovskite unit cell and perovskite nanoplatelets with the chemical species used in this study. The parameter *n* indicates the number of lead halide octahedral layers in the direction of nanoplatelet thickness. (b) Schematic illustration of nanoplatelet synthesis procedure. (c) Solution phase photoluminescence and absorption spectra of colloidal *n* = 2 MAPbBr nanoplatelets in toluene. (d) X-ray diffraction (XRD) pattern of a drop-cast *n* = 2 MAPbBr nanoplatelet film. (e) Scanning electron microscopy (SEM) image and (f) Transmission electron microscopy (TEM) image of *n* = 2 MAPbBr nanoplatelets.

Colloidal perovskite nanoplatelets (Chemical formula: $L_2[ABX_3]_{n-1}BX_4$ where *n* refers to the number of octahedral $[BX_6]^{4-}$ layers in the direction of confinement) were synthesized by a previously reported ligand-assisted reprecipitation method[34] with slight modifications. Methylammonium (MA) and formamidinium (FA) were used as A-site organic cations in this study, with lead (Pb) as B-site metal cation, and bromide (Br) and iodide (I) as halide anions. For better colloidal stability and thickness control of nanoplatelets, a 1:1 mixture of butylammonium (BA) and octylammonium (OA) were incorporated as ligands (Figure 1a).[34]

Schematic illustration in Figure 1b shows the synthesis procedure. First, precursor salts (AX, BX_2 and LX) were dissolved and precursor solutions were mixed in the desired ratio for specific target thickness. Lastly, this mixed precursor solution was dropped into toluene and perovskite nanoplatelets were crystallized due to the abrupt change in solubility. Further details are included under Experimental Methods.

Through this method, colloidal *n* = 2 methylammonium lead bromide (MAPbBr) nanoplatelets that emit in deep-blue range (λ_{max} = 437 nm) with narrow full-width-at-half-maximum (FWHM = 14 nm) and small Stokes shift (4 nm) (Figure 1c) were synthesized. When dropcast, the nanoplate-

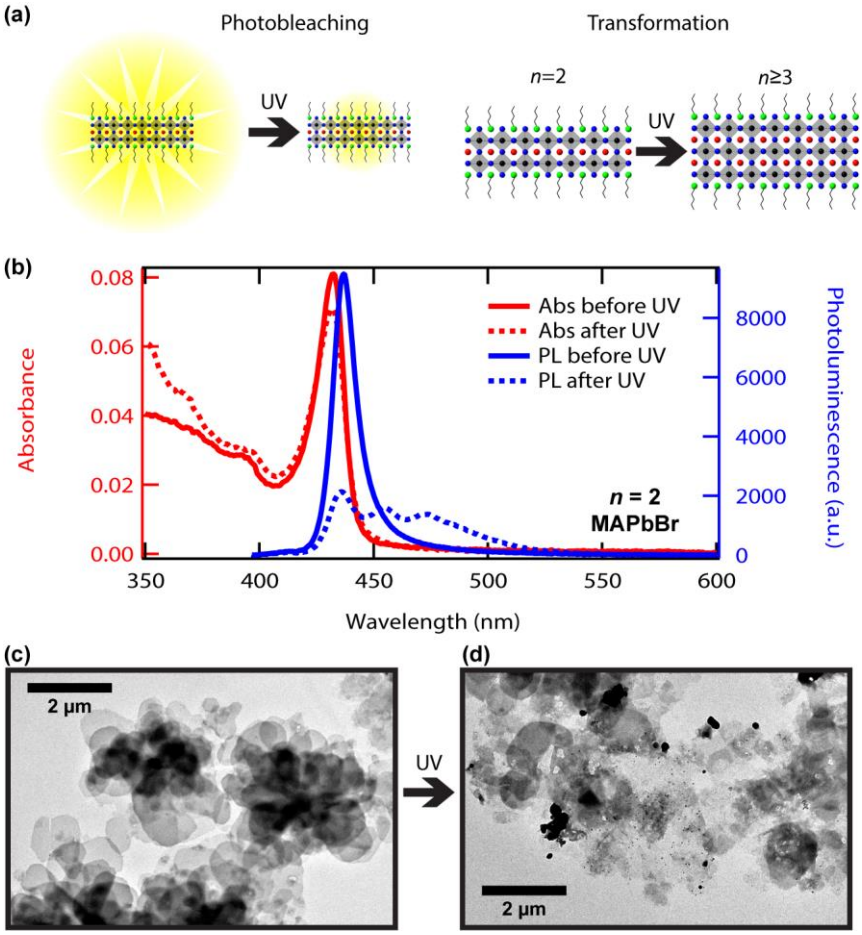

Figure 2. *Photoinstability of lead halide perovskite nanoplatelets.* (a) Schematic illustrations of two changes that nanoplatelets suffer under UV irradiation. (b) Photoluminescence and absorption spectra of colloidal n = 2 MAPbBr nanoplatelets in toluene before and after UV irradiation under air. (365 nm, 180 mW/cm^2, 1 hour) (c-d) TEM image of n = 2 MAPbBr nanoplatelets before and after UV irradiation.

lets preferentially lay flat on the substrate with a stacking periodicity of 2.2 nm, as seen by the periodic stacking peaks[34, 50] at integer multiples of 3.9º observed in the X-ray diffraction (XRD) pattern (Figure 1d). The nanoplatelets, which have lateral dimension ranging from 0.5-5 µm (Figure 1e-f), appear to be dispersed as individual sheets in the colloidal solution based on contrast in transmission electron microscopy (TEM) images (Figure 1f).

Classifying Types of Photoinstability

In Figure 2a, we categorize the two photoinstability phenomena that nanoplatelets suffer under UV irradiation, namely *photobleaching* and *transformation*. As seen in figure 2b, PL from n = 2 MAPbBr nanoplatelets at 437 nm was greatly reduced after UV irradiation ("photobleaching"). Additionally, PL emission peaks from thicker perovskite structures appeared at 455 nm and 474 nm, which are believed to come from small amounts of n = 3 and n = 4 structures that were formed during UV irradiation ("transformation").[38] However, the decrease of the excitonic feature at 433 nm in the absorption spectrum was less extensive than the 77% decrease in the n = 2 PL peak intensity after UV irradiation. Furthermore, it is noteworthy that only the n = 2 excitonic feature, but not n = 3 or n = 4 features (which should appear at ~450 nm and ~470 nm respectively),[38] was observed in the absorption spectrum after UV irradiation. To test for a change in Pb oxidation state (signifying different chemical bonding in the sample), we characterized the freshly prepared and irradiated samples with X-ray photoelectron spectroscopy (XPS, Figure S5) but no significant change was observed.

Transmission electron microscopy (TEM) images in Figure 2c and Figure 2d show the structure of nanoplatelets before and after UV exposure (More images in Figure S3). In Figure 2c, individual nanoplatelets could be easily distinguished and identified, although they were mostly stacked together presumably due to high surface-to-volume ratio. As shown in Figure 2d, it became difficult to distinguish individual nanoplatelets once irradiated; we also observed regions of strong TEM contrast in regions smaller than the lateral dimension of the nanoplatelets (~1 µm), possibly revealing thickness variations within individual nanoplatelets or degradation products.

Based on the observed changes to the absorption and photoluminescence spectra and TEM structural imaging, we conclude that photobleaching arises from *both* degradation of a portion of the nanoplatelet dispersion and a reduction in the intrinsic PLQY of the remaining nanoplatelets. Additionally, some of the n = 2 nanoplatelet structures are transformed into less-confined (n = 3 and n = 4 in this case) structures either by structural rearrangement within a single nanoplatelet or by merging of multiple nanoplatelets. Downhill energy transfer from thinner (higher-energy) to thicker (lower-energy) struc-

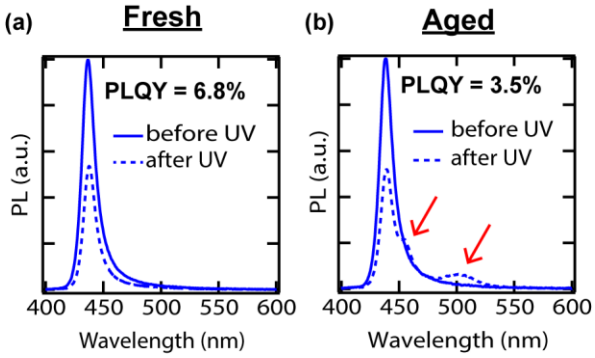

Figure 3. *Effects of the precursor solution aging.* PLQY of as synthesized colloidal n = 2 MAPbBr nanoplatelets in toluene and solution phase photoluminescence spectra before and after UV irradiation (365 nm, 24 mW/cm^2, 1 hour) under air, when (a) freshly prepared and (b) 2-months-aged precursor solutions were used.

tures combined with higher PLQY of thicker structures can amplify the contribution of redshifted emitters in the ensemble PL spectrum, as we observed in Figure 2b. Low enthalpy of formation for perovskites[55] combined with facile ionic migration[56] is believed to facilitate the transformation of nanoplatelets into thicker structures in solution. Although slight redshift of PL under UV have already been observed in perovskite quantum dots (QDs),[57] this transformation behavior can be especially problematic for strongly quantum-confined atomically- thin nanoplatelets because slight change in the thickness induce dramatic changes to the ensemble optical properties.

Effect of Precursor Solution Aging

To investigate the role of precursor aging, we prepared nanoplatelets using two different sets of precursor solutions. One set of precursors was prepared fresh, while the other was stored inside a nitrogen (N_2) glovebox for two months before use. Figure 3 shows PLQY and PL spectra of n = 2 MAPbBr nanoplatelet dispersions prepared from fresh and aged precursor solutions. In Figure 3a, n = 2 MAPbBr nanoplatelets synthesized from freshly prepared precursor solutions showed solution phase PLQY of 6.8% and did not transform into thicker structures after moderate UV irradiation (24 mW/cm^2) under air for 1 hour. On the other hand, when synthesized from aged precursors, PLQY dropped to 3.5% and PL from n = 3 structures at 455 nm as well as the bulk-like emission around 500 nm appeared, as indicated by the red arrows in Figure 3b. Thus, it becomes evident that the aging of individual perovskite precursors even under a N_2 atmosphere affects stability and PLQY of the resultant nanoplatelets.

To explain this precursor aging effect, the first possibility considered was the formation of impurities through slow reaction between alkylammonium bromide and DMF. Among MABr, BABr and OABr, MABr was chosen as a representative of alkylammonium bromide species because of low steric hindrance and high reactivity. Fourier-transform infrared (FTIR) spectroscopy and ^{1}H nuclear magnetic resonance (NMR) spectroscopy were employed to detect the presence of any potential reaction products formed in the MABr/DMF precursor solution after aging in N_2 atmosphere for 0 days (fresh), 2 days, 2.5 months, and 3.5 months. However, no significant difference in the FTIR spectrum was observed (Figure S6). Ammonium and methyl proton peaks were observed in the ^{1}H NMR spectrum at 8.11-8.20 ppm and 2.68-2.70 ppm, respectively (Figure S6), as expected from previous studies.[58] However, there was no correlation with precursor aging time. Instead, these shifts arise from differing concentrations of water present during NMR sample preparation (see Supporting Information). Furthermore we did not observe the appearance of new peaks from side reactions via ^{1}H NMR. Consequently, the presence of side products from alkylammonium salts reacting with DMF was ruled out.

A second possible origin of the precursor aging effect that was considered is a change in the size distribution of lead polyhalide colloids in DMF. It has been reported that lead halide exists as lead polyhalide colloids in DMF[59-61] (i.e. $[PbX_3]^-$, $[PbX_4]^{2-}$, $[PbX_5]^{3-}$ and $[PbX_6]^{4-}$) and the size distribution affects crystallization kinetics during spin-coating perovskite precursor solutions in DMF, further affecting the quality of spin-coated perovskite crystal film.[62] To test whether similar behavior might be occurring in our reprecipitation synthesis, we performed dynamic light scattering (DLS) measurements to compare the colloidal size distribution of freshly prepared and 2-month-old $PbBr_2$ solutions in DMF. Clear changes to the size distribution before and after aging were evident in the DLS autocorrelation decay profile (Figure S7), but large scan-to-scan variation made a quantitative analysis difficult. Though these measurements suggest that the presence of lead polyhalide colloids in the precursor solution affects the photostability of resulting nanoplatelets, the mechanism for this effect is not understood.

Effect of Perovskite Composition

In Figure 4, we present data showing how composition of nanoplatelets affects photostability under air. Four different colloidal nanoplatelet solutions, n = 2 FAPbBr, n = 2 MAPbBr, n = 2 FAPbI and n = 2 MAPbI, were synthesized and UV-irradiated under air while stirring in toluene. To induce fast and dramatic change, extreme UV power density (λ = 365 nm, 180 mW/cm^2) was used. Because lead and halide ions mainly contribute to the formation of band edge electronic states,[19] both MAPbX and FAPbX nanoplatelets have similar PL emission at 437 nm for X=Br and at 575 nm for X=I. In the n = 2 FAPbBr solution (Figure 4a), PL from bulk-like ($n \geq 6$) structures appeared immediately upon UV exposure, along with photobleaching of the n = 2 PL peak at 437 nm. On the other hand, photobleaching of the primary n = 2 peak was mainly observed for the first 20 minutes of UV irradiation in n = 2 MAPbBr nanoplatelets, followed eventually by the slow appearance of PL peaks from n = 3 and n = 4 structures (Figure 4b). The iodide n = 2 analogues showed similar photobleaching behavior as their bromide counterparts, as shown in Figure 4c and Figure 4d. Interestingly, weak blue-shifted PL at 512 nm (n = 1) appeared between 10 and 20 minutes of UV irradiation for both MAPbI and FAPbI, but no emission from thicker structures was observed.

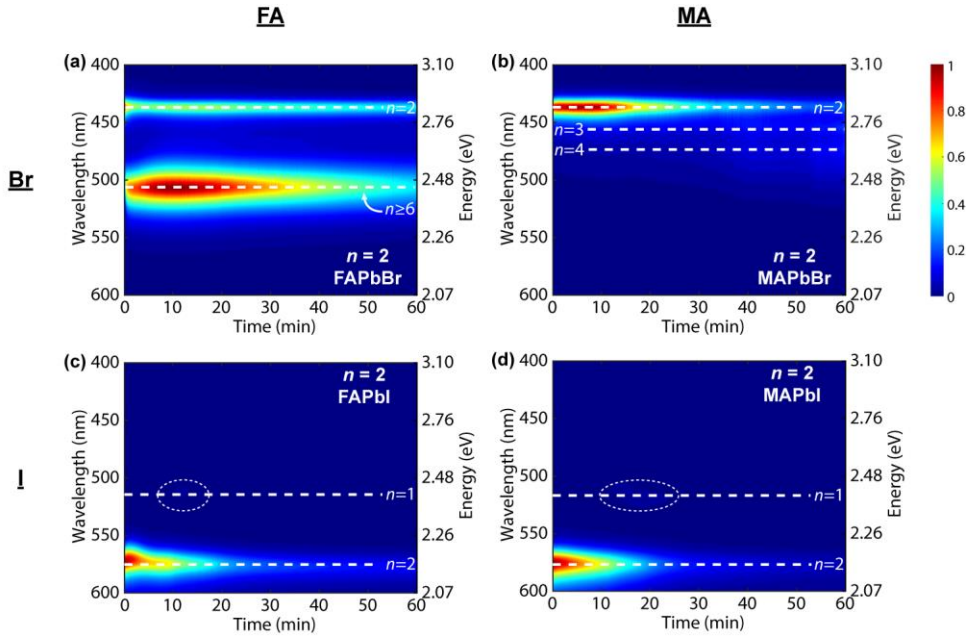

Figure 4. *Photoluminescence stability under air*. (a-d) Evolution of photoluminescence spectra under UV irradiation (365 nm, 180 mW/cm^2) for colloidal n = 2 FAPbBr, n = 2 MAPbBr, n = 2 FAPbI and n = 2 MAPbI nanoplatelets in toluene under air. (White dotted lines indicate the peak positions for nanoplatelets with corresponding compositions and thicknesses.)

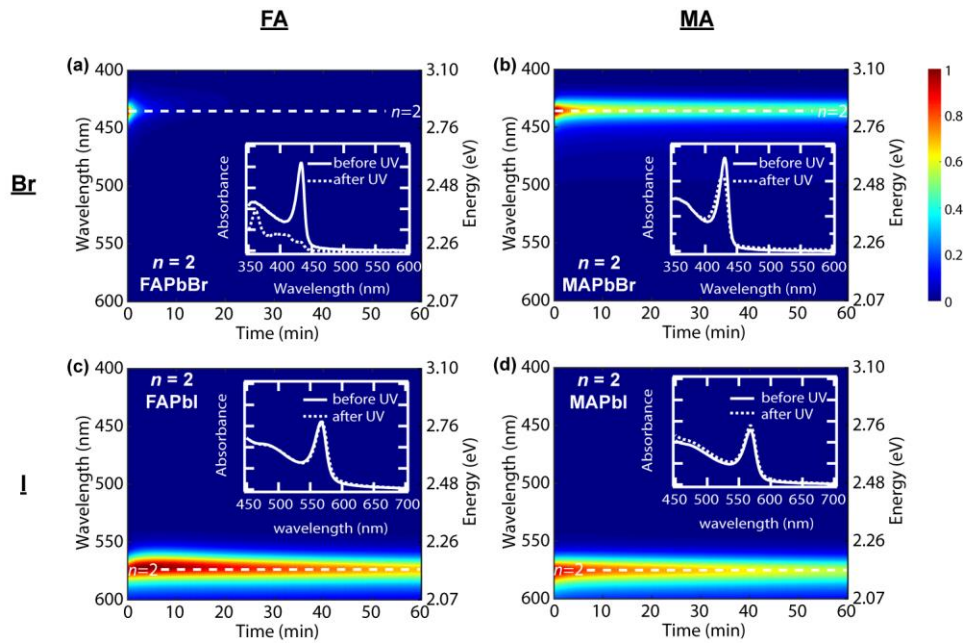

Figure 5. *Photoluminescence stability under N_2*. (a-d) Evolution of photoluminescence spectra under UV irradiation (365 nm, 180 mW/cm^2) for colloidal n = 2 FAPbBr, n = 2 MAPbBr, n = 2 FAPbI and n = 2 MAPbI nanoplatelets in toluene under N_2. (Insets: Absorption spectra before and after UV irradiation. White dotted lines indicate the peak positions for nanoplatelets with corresponding compositions.)

In Figure 5, we show the effect of UV irradiation on colloidal nanoplatelet solutions under N_2 atmosphere. Whereas n = 2 MAPbBr nanoplatelets partially maintained their PL intensity after 1 hour of exposure to UV (Figure 5b), n = 2 FAPbBr nanoplatelets completely lost PL intensity in a few minutes under UV irradiation (Figure 5a). It is also noteworthy that photobleaching behaviors of n = 2 MAPbI and n = 2 FAPbI nanoplatelets under N_2 were similar (Figure 5c and Figure 5d), as they also were under air (Figure 4c and Figure 4d). Furthermore, transformation to n = 1 or n > 2 structures was not observed in any of the four colloidal nanoplatelet dispersions irradiated under N_2, although they each demonstrated varying degrees of photobleaching. Note that in Figure 5b-d, while nanoplatelet PL intensity significantly dropped, corresponding excitonic features in the absorption spectra did not decrease nearly as much. This again demonstrates that photobleaching is not solely due to a drop in PLQY nor degradation of nanoplatelets, but rather a combination of the two.

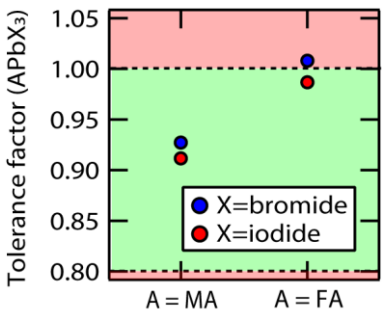

Figure 6. Tolerance factors of lead halide perovskites.

Comparing the changes during UV irradiation under air (Figure 4) and under N_2 (Figure 5), we conclude that photobleaching results from an intrinsic instability of the perovskite nanoplatelet against photoexcitation, whereas transformation of nanoplatelets to thicker or thinner structures requires the participation of an extrinsic chemical species present in air (discussed below). We note that no changes to the PL spectrum were observed when the nanoplatelet solution was irradiated with sub-bandgap light of similar intensity at 785 nm (Figure S9).

We hypothesize that the intrinsic instability of perovskite nanoplatelets under UV photoexcitation can be correlated with the structural stability of the underlying perovskite lattice. Goldschmidt's tolerance factor, defined as $\frac{r_A+r_X}{\sqrt{2}(r_B+r_X)}$ where r_A, r_B and r_X denotes ionic radii of A, B and X ions, respectively, is one parametrization of the structural stability of the perovskite lattice.[63] A stable perovskite structure is predicted to form when the tolerance factor lies between 0.8 and 1[64], and tuning the tolerance factor to enhance the stability is a popular technique in the field of perovskite solar cells.[18, 65-67] Figure 6 shows the tolerance factors of relevant bulk lead halide perovskites calculated from ionic radii values reported by Kieslich *et al*.[68] Although it has been reported that slight lattice relaxation occurs for two-dimensional nanoplatelets[69] compared to bulk perovskites, we expect tolerance factors of nanoplatelets to be similar to bulk perovskites. From Figures 4 and 5, we observed that n = 2 FAPbBr nanoplatelets were least stable compared to n = 2 MAPbBr, n = 2 FAPbI and n = 2 MAPbI. As shown in Figure 6, n = 2 FAPbBr has the largest tolerance factor, at the limit of the stable range for the perovskite structure. Considering that perovskites with large tolerance factors tend to relieve strain by forming defect vacancies[66] and defects in perovskite crystal can propagate,[70] we believe that structural instability of n = 2 FAPbBr nanoplatelets may be one of the main causes of such instability under UV irradiation. Also, it has been reported that larger dipole moment of MA compared to FA (2.3D for MA, 0.2D for FA) enables MA to more readily respond to the presence of charge carriers upon electronic excitations.[71] In our systems, less facile reorientation of FA within nanoplatelets, compared to MA, may result in less effective charge carrier screening and enhanced distortion of crystal lattices. This can also contribute to the inferior stability of n = 2 FAPbBr nanoplatelets. On the other hand, both n = 2 MAPbI and n = 2 FAPbI nanoplatelets have tolerance factors within the range where perovskite structures are stable and this could explain why substituting A-site cation from FA to MA does not significantly affect the photostability of iodide nanoplatelets, unlike bromide counterparts.

Water is the Source of Extrinsic Photoinstability

To identify the external chemical species responsible for the transformation of nanoplatelets into thicker or thinner structures under UV irradiation, we performed the same experiments shown in Fig.4 and Fig. 5 under three different controlled environments: *dry air*, *dry nitrogen*, and *humid nitrogen*. In Figure 7a and Figure 7b, colloidal n = 2 MAPbBr solutions in toluene were irradiated with UV light (λ = 365 nm, 180 mW/cm^2) while kept under either dry air with 2.6% relative humidity (RH) or dry N_2 with <0.3 ppm H_2O, respectively. Both data sets show similar photobleaching behavior without significant redshifted emission from thicker structures. In contrast, when the nanoplatelet solution was irradiated under humid N_2 (RH 80%), n = 3 and n = 4 emission appeared within 10 minutes and 20 minutes, respectively (Figure 7c). These results confirm that moisture participates in the transformation of nanoplatelets to different-thickness structures, whereas photobleaching occurs regardless of the presence of oxygen or water.

We note that the equilibrium solubility of H_2O in toluene is low (0.0270 mol/L at 25ºC)[72] but its effect, shown in Fig. 7, is clear. Perovskites are dissolvable in polar solvents, including water, so it is not unexpected that H_2O could assist ion rearrangement within the lattice. Photoexcitation shifts charge density from halide anions to Pb cations,[73] which is believed to weaken hydrogen bonds between halide and alkylammonium ions. Together with deprotonation of alkylammonium ions by water molecules,[74] light and H_2O can act synergestically to accelerate structural transformation in perovskite nanoplatelets.

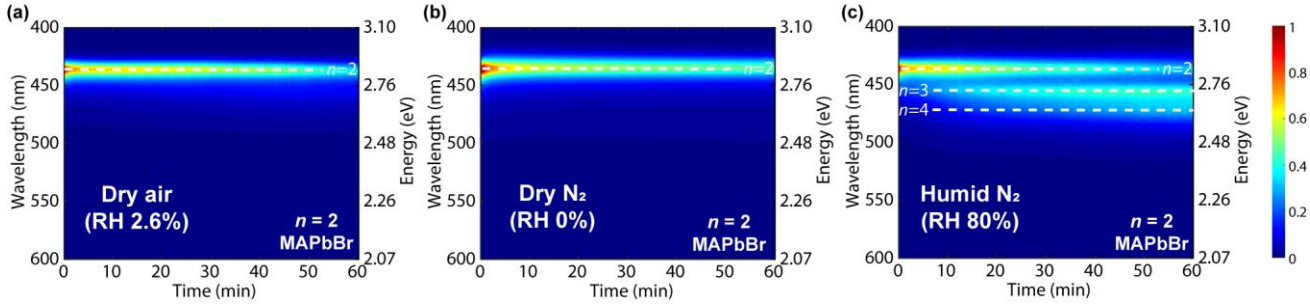

Figure 7. *Separating the effects of oxygen and moisture.* (a-c) Evolution of photoluminescence spectra under UV irradiation (365 nm, 180 mW/cm^2) for colloidal n = 2 MAPbBr nanoplatelets in toluene under dry air, dry N_2 and humid N_2. (White dotted lines indicate the peak positions for nanoplatelets with corresponding thicknesses.)

Table 1. *Formulations for n = 2 MAPbBr nanoplatelets (NPLs) with varied amount of ligands.*

	MABr	**$PbBr_2$**	**BABr**	**OABr**
Stoichiometric ratio ($L_2[MAPbBr_3]PbBr_4$)	1	2	1	1
'2.5x ligands'	1	2	2.5	2.5
'5x ligands' (Standard procedure for *n* = 2 NPLs)	1	2	5	5
'10x ligands'	1	2	10	10

Note: Numbers indicate the volumetric ratios of individual precursor solutions (0.2M) in the mixed precursor solutions. For example, to prepare the precursor solution for *n* = 2 MAPbBr ($L_2[MAPbBr_3]PbBr_4$) 5x ligands sample, 0.2M MABr, $PbBr_2$, BABr and OABr solutions were mixed in the volumetric ratio of 1:2:5:5. Full names of chemical species can be found in 'Abbreviation' section.

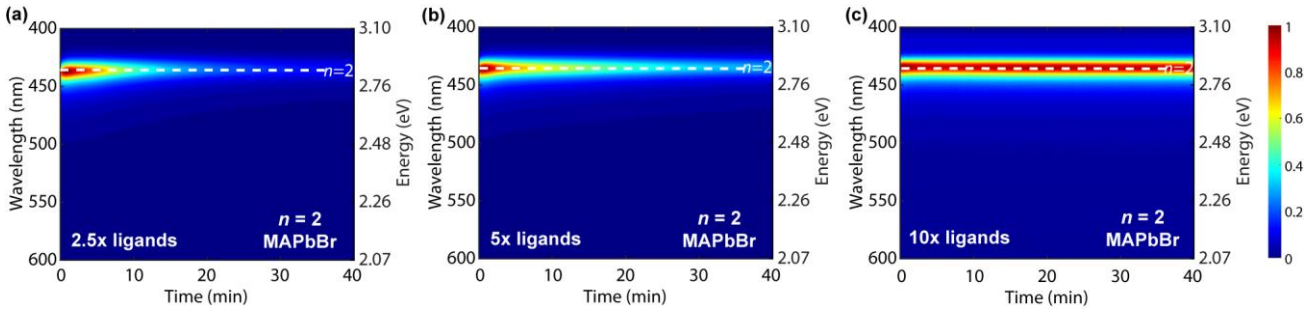

Figure 8. *Excess ligands improve intrinsic photostability in solution.* (a-c) Evolution of photoluminescence spectra under UV irradiation (365 nm, 180 mW/cm^2) for colloidal *n* = 2 MAPbBr nanoplatelets in toluene with varied amounts of excess ligands under N_2. (White dotted lines indicate the peak positions for *n* = 2 MAPbBr nanoplatelets.)

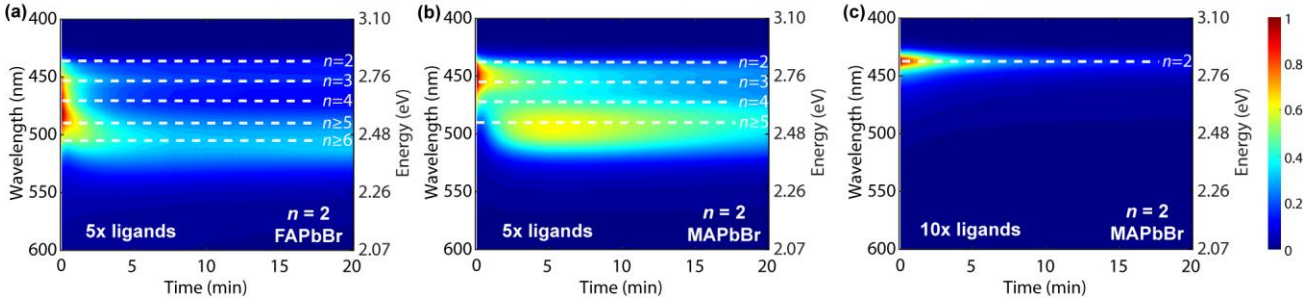

Figure 9. *Excess ligands suppress transformation in thin films.* Evolution of photoluminescence spectra under UV irradiation (365 nm, 120 mW/cm^2) in air for (a) *n* = 2 FAPbBr 5x ligands film (b) *n* = 2 MAPbBr 5x ligands film (c) *n* = 2 MAPbBr 10x ligands film (White dotted lines indicate the peak positions for nanoplatelets with corresponding thicknesses.)

Enhancing the Stability by Adding Excess Ligand

The effect of adding excess alkylammonium ligands was investigated as a strategy for improving nanoplatelet photostability.[38] Three *n* = 2 MAPbBr nanoplatelet solutions were prepared with different relative amounts of alkylammonium bromide ligands in mixed precursor solutions (Table 1). As shown in Figure 8, the extent of photobleaching was reduced as greater ligand excess was added to the mixed precursor solution (Figure 8a-Figure 8c). Furthermore, colloidal *n* = 2 MAPbBr nanoplatelets synthesized with 10x ligands showed remarkable photostability, preserving 95% of PL intensity even after 40 minutes of intense UV irradiation under N_2. This effect is attributed to two factors: 1) more saturated surface coverage in the presence of excess alkylammonium ligands, given the dynamic nature of ligand binding in perovskite nanocrystals,[75] and 2) increased structural robustness of perovskite layers in the presence of excess bromide ions,[38, 50] which prevents the formation of harmful bromide defect vacancies.[76] Interestingly, no significant enhancement in PLQY was observed with ligand excess (Figure S11), unlike several

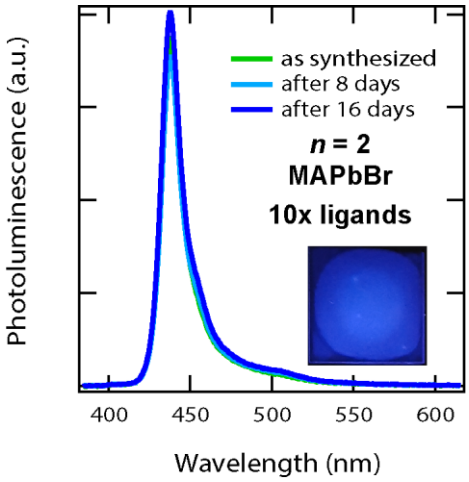

Figure 10. *Stability of n = 2 MAPbBr 10x ligands film under ambient conditions.* (Inset: Image showing deep-blue luminescence from dropcast *n* = 2 MAPbBr 10x ligands film.)

previous reports[38, 50] where stability enhancement was accompanied by PLQY increase.

Ligand excess was also found to improve the stability of dropcast nanoplatelet films. Obtaining pure n = 2 deep-blue emission from dropcast n = 2 MAPbBr nanoplatelets synthesized by the reprecipitation method is challenging in general. To prepare dropcast nanoplatelet films, the colloidal nanoplatelet dispersion is centrifuged, redispersed, dropcasted and dried – processes that can induce transformation and degradation. Furthermore, efficient energy transfer within nanoplatelet films along with higher PLQY of thicker nanoplatelets can amplify the contribution of minority red-shifted structures to the overall photoluminescence spectrum. As shown in Figure 9a and Figure 9b, dropcast films of n = 2 FAPbBr (5x ligands) and n = 2 MAPbBr (5x ligands) showed not only n = 2 emission at 437 nm, but also emission from n = 3 and thicker structures in the initial PL spectrum. Upon further UV irradiation, redshifted emission from bulk-like structures at λ > 500 nm dominated the PL spectrum and eventual photobleaching was observed. However, XRD showed no noticeable change after irradiation, suggesting that thicker structures exist in small amounts and n = 2 nanoplatelets are still the majority species (Figure S12), while downhill energy funneling and higher emission efficiency of thicker nanoplatelets potentially making red-shifted emission pronounced. On the other hand, n = 2 MAPbBr 10x ligand films showed pure n = 2 deep-blue luminescence when dropcast and the PL spectrum did not red-shift over time under UV in air, though photobleaching did occur (Fig. 9c). Moreover, the dropcast n = 2 MAPbBr 10x ligand film also showed superior stability under ambient conditions as shown in Figure 10. Despite small fluctuations between the measurements, deep-blue luminescence from the film essentially maintained its PL intensity for more than two weeks when the film was stored under ambient conditions. Enhanced robustness of the nanoplatelets and a stronger barrier to moisture diffusion through the surface ligand layer are believed to be the key factors for this dramatic stability enhancement.

Finally, we note that there have been several published reports on varying degrees of nanoplatelet stability.[34-35, 38, 50, 53] As we discussed, nanoplatelet stability depends not only on intrinsic material properties (cation species, structural robustness, surface ligands coverage, etc.) but also on external factors such as irradiation power density (Figure S13), presence of air and relative humidity. In some cases, lack of detailed reporting of this information makes direct comparison of results from different laboratories difficult. Greater collective effort in reporting such details will accelerate the development of the field.

Conclusions

In this work, we characterized the photostability of colloidal n = 2 methylammonium and formamidinium lead bromide nanoplatelets in toluene solution and in thin film. We identified signatures of nanoplatelet degradation, PLQY loss, and transformation into different-thickness structures. Furthermore, we showed that the usage of freshly prepared precursor solutions, substitution of organic cations, complete isolation from moisture, and the addition of excess alkylammonium bromide ligands can be effective strategies to enhance the photostability of n = 2 lead bromide perovskite nanoplatelets. By applying those tactics, we could prepare a deep-blue luminescent perovskite nanoplatelet film which was stable under ambient conditions and did not transform under air and UV exposure. In future studies, the chemical pathways of nanoplatelet degradation and mechanisms of structural transformation will need to be addressed, along with detailed investigation on how precursor solution aging affects nanoplatelet properties. While we have identified some strategies for improving nanoplatelet stability, further improvement is needed before these materials will become viable in commercial technologies.

ASSOCIATED CONTENT

Supporting Information.
Details on chemicals and nanoplatelet synthesis, pictures of colloidal nanoplatelet solutions, TEM images, XPS spectra, FTIR spectra, NMR spectra, DLS data, absorption spectra, photoluminescence stability under sub-bandgap light, photoluminescence stability of n = 1 nanoplatelets, PLQY of nanoplatelets, XRD patterns before and after UV irradiation, power-dependent photobleaching behavior.

AUTHOR INFORMATION

Corresponding Author

* E-mail: tisdale@mit.edu

ORCID

Seung Kyun Ha: 0000-0003-2967-1097
Catherine M. Mauck: 0000-0002-6432-9724
William A. Tisdale: 0000-0002-6615-5342

Author Contributions

The manuscript was written through contributions of all authors. All authors have given approval to the final version of the manuscript.

Funding Sources

U.S. DOE (DE-SC0001088)
U.S. DOE (DE-SC0019345)

Notes

The authors declare no completing financial interest.

ACKNOWLEDGMENT

The authors thank Wenbi Shcherbakov-Wu for performing FTIR measurements; Helen Yao, Carolyn Mills and Prof. Bradley Olsen for DLS data acquisition; Elisabeth Shaw for performing XPS measurement; and Nicholas Morgante and Watcharaphol Paritmongkol for experimental assistance in the early stage of the project. Nanoplatelet synthesis and structural characterization was supported as part of the Center for Excitonics, and Energy Frontier Research Center funded by the U.S. Department of Energy, Office of Science, Basic Energy Sciences (BES) under award number DE-SC0001088 (MIT). Optical characterization and photostability investigations were supported by the U.S. Department of Energy, Office of Science, Basic Energy Sciences (BES) under award number DE-SC0019345. Seung Kyun Ha was partially supported by the Kwanjeong Education Foundation Overseas Doctoral Program Scholarship and Catherine M. Mauck was supported by the Camille and Henry Dreyfus Foundation Postdoctoral Program in Environmental Chemistry. This work made use of the MRSEC Shared Experimental Facilities at MIT, supported by the National Science Foundation under award number DMR-08-19762, and the Department of Chemistry Instrumentation Facility (DCIF) at MIT.

ABBREVIATIONS

MA, methylammonium; FA, formamidinium; Pb, lead; Br, bromide; I, iodide; BA, butylammonium; OA, octylammonium; PL, photoluminescence; PLQY, photoluminescence quantum yield; FTIR, Fourier transform infrared spectroscopy; NMR, ^{1}H nuclear magnetic resonance; TEM, transmission electron microscopy; SEM, scanning electron microscopy; XRD, X-ray diffraction; XPS, X-ray photoelectron spectroscopy; DLS, dynamic light scattering.

REFERENCES

1. Bourzac, K., Quantum dots go on display. *Nature* **2013,** *493* (7432), 283.
2. Yang, X.; Xu, X.; Zhou, G., Recent advances of the emitters for high performance deep-blue organic light-emitting diodes. *J. Mater. Chem. C* **2015,** *3* (5), 913-944.
3. Im, Y.; Byun, S. Y.; Kim, J. H.; Lee, D. R.; Oh, C. S.; Yook, K. S.; Lee, J. Y., Recent Progress in High-Efficiency Blue-Light-Emitting Materials for Organic Light-Emitting Diodes. *Adv. Funct. Mater.* **2017,** *27* (13), 1603007.
4. Shirasaki, Y.; Supran, G. J.; Bawendi, M. G.; Bulović, V., Emergence of colloidal quantum-dot light-emitting technologies. *Nat. Photonics* **2012,** *7* (1), 13-23.
5. Dai, X.; Deng, Y.; Peng, X.; Jin, Y., Quantum-Dot Light-Emitting Diodes for Large-Area Displays: Towards the Dawn of Commercialization. *Adv. Mater.* **2017,** *29* (14), 1607022.
6. Shirasaki, Y.; Supran, G. J.; Tisdale, W. A.; Bulović, V., Origin of efficiency roll-off in colloidal quantum-dot light-emitting diodes. *Phys. Rev. Lett.* **2013,** *110* (21), 217403.
7. Verzellesi, G.; Saguatti, D.; Meneghini, M.; Bertazzi, F.; Goano, M.; Meneghesso, G.; Zanoni, E., Efficiency droop in InGaN/GaN blue light-emitting diodes: Physical mechanisms and remedies. *J. Appl. Phys.* **2013,** *114* (7), 10_1.
8. Kim, H. S.; Lee, C. R.; Im, J. H.; Lee, K. B.; Moehl, T.; Marchioro, A.; Moon, S. J.; Humphry-Baker, R.; Yum, J. H.; Moser, J. E.; Gratzel, M.; Park, N. G., Lead iodide perovskite sensitized all-solid-state submicron thin film mesoscopic solar cell with efficiency exceeding 9%. *Sci. Rep.* **2012,** *2*, 591.
9. Zhou, H.; Chen, Q.; Li, G.; Luo, S.; Song, T.-b.; Duan, H.-S.; Hong, Z.; You, J.; Liu, Y.; Yang, Y., Interface engineering of highly efficient perovskite solar cells. *Science* **2014,** *345* (6196), 542-546.
10. Wilks, R. G.; Bär, M., Perovskite solar cells: Danger from within. *Nat. Energy* **2017,** *2* (1), 16204.
11. Yang, W. S.; Park, B.-W.; Jung, E. H.; Jeon, N. J.; Kim, Y. C.; Lee, D. U.; Shin, S. S.; Seo, J.; Kim, E. K.; Noh, J. H.; Seok, S. I., Iodide management in formamidinium-lead-halide−based perovskite layers for efficient solar cells. *Science* **2017,** *356* (6345), 1376-1379.
12. Saidaminov, M. I.; Abdelhady, A. L.; Murali, B.; Alarousu, E.; Burlakov, V. M.; Peng, W.; Dursun, I.; Wang, L.; He, Y.; Maculan, G.; Goriely, A.; Wu, T.; Mohammed, O. F.; Bakr, O. M., High-quality bulk hybrid perovskite single crystals within minutes by inverse temperature crystallization. *Nat. Commun.* **2015,** *6*, 7586.
13. Ma, L.; Hao, F.; Stoumpos, C. C.; Phelan, B. T.; Wasielewski, M. R.; Kanatzidis, M. G., Carrier diffusion lengths of over 500 nm in lead-free perovskite CH3NH3SnI3 films. *J. Am. Chem. Soc.* **2016,** *138* (44), 14750-14755.
14. Stranks, S. D.; Eperon, G. E.; Grancini, G.; Menelaou, C.; Alcocer, M. J. P.; Leijtens, T.; Herz, L. M.; Petrozza, A.; Snaith, H. J., Electron-Hole Diffusion Lengths Exceeding 1 Micrometer in an Organometal Trihalide Perovskite Absorber. *Science* **2013,** *342* (6156), 341-344.
15. Dong, Q.; Fang, Y.; Shao, Y.; Mulligan, P.; Qiu, J.; Cao, L.; Huang, J., Electron-hole diffusion lengths> 175 µm in solution grown CH3NH3PbI3 single crystals. *Science* **2015,** *347* (6225), 967-970.
16. Shi, D.; Adinolfi, V.; Comin, R.; Yuan, M.; Alarousu, E.; Buin, A.; Chen, Y.; Hoogland, S.; Rothenberger, A.; Katsiev, K.; Losovyj, Y.; Zhang, X.; Dowben, P. A.; Mohammed, O. F.; Sargent, E. H.; Bakr, O. M., Low trap-state density and long carrier diffusion in organolead trihalide perovskite single crystals. *Science* **2015,** *347* (6221), 519-522.
17. Saliba, M.; Matsui, T.; Seo, J. Y.; Domanski, K.; Correa-Baena, J. P.; Nazeeruddin, M. K.; Zakeeruddin, S. M.; Tress, W.; Abate, A.; Hagfeldt, A.; Gratzel, M., Cesium-containing triple cation perovskite solar cells: improved stability, reproducibility and high efficiency. *Energy Environ. Sci.* **2016,** *9* (6), 1989-1997.
18. McMeekin, D. P.; Sadoughi, G.; Rehman, W.; Eperon, G. E.; Saliba, M.; Horantner, M. T.; Haghighirad, A.; Sakai, N.; Korte, L.; Rech, B.; Johnston, M. B.; Herz, L. M.; Snaith, H. J., A mixed-cation lead mixed-halide perovskite absorber for tandem solar cells. *Science* **2016,** *351* (6269), 151-155.
19. Kovalenko, M. V.; Protesescu, L.; Bodnarchuk, M. I., Properties and potential optoelectronic applications of lead halide perovskite nanocrystals. *Science* **2017,** *358* (6364), 745-750.
20. Akkerman, Q. A.; Rainò, G.; Kovalenko, M. V.; Manna, L., Genesis, challenges and opportunities for colloidal lead halide perovskite nanocrystals. *Nat. Mater.* **2018,** *17*, 394−405.
21. Protesescu, L.; Yakunin, S.; Bodnarchuk, M. I.; Krieg, F.; Caputo, R.; Hendon, C. H.; Yang, R. X.; Walsh, A.; Kovalenko, M. V., Nanocrystals of Cesium Lead Halide Perovskites (CsPbX(3), X = Cl, Br, and I): Novel Optoelectronic Materials Showing Bright Emission with Wide Color Gamut. *Nano Lett.* **2015,** *15* (6), 3692-3696.
22. Schmidt, L. C.; Pertegas, A.; Gonzalez-Carrero, S.; Malinkiewicz, O.; Agouram, S.; Minguez Espallargas, G.; Bolink, H. J.; Galian, R. E.; Perez-Prieto, J., Nontemplate synthesis of CH3NH3PbBr3 perovskite nanoparticles. *J. Am. Chem. Soc.* **2014,** *136* (3), 850-853.
23. Zhang, F.; Zhong, H.; Chen, C.; Wu, X.-g.; Hu, X.; Huang, H.; Han, J.; Zou, B.; Dong, Y., Brightly Luminescent and Color-Tunable Colloidal CH3NH3PbX3 (X = Br, I, Cl) Quantum Dots: Potential Alternatives for Display Technology. *ACS Nano* **2015,** *9* (4), 4533-4542.
24. Dong, Y.; Qiao, T.; Kim, D.; Parobek, D.; Rossi, D.; Son, D. H., Precise Control of Quantum Confinement in Cesium Lead Halide Perovskite Quantum Dots via Thermodynamic Equilibrium. *Nano Lett.* **2018,** *18* (6), 3716-3722.
25. Zheng, K.; Zhu, Q.; Abdellah, M.; Messing, M. E.; Zhang, W.; Generalov, A.; Niu, Y.; Ribaud, L.; Canton, S. E.; Pullerits, T., Exciton binding energy and the nature of emissive states in organometal halide perovskites. *J. Phys. Chem. Lett.* **2015,** *6* (15), 2969-2975.
26. Saidaminov, M. I.; Mohammed, O. F.; Bakr, O. M., Low-Dimensional-Networked Metal Halide Perovskites: The Next Big Thing. *ACS Energy Lett.* **2017,** *2* (4), 889-896.
27. Pan, J.; Shang, Y.; Yin, J.; De Bastiani, M.; Peng, W.; Dursun, I.; Sinatra, L.; El-Zohry, A. M.; Hedhili, M. N.; Emwas, A. H.; Mohammed, O. F.; Ning, Z.; Bakr, O. M., Bidentate Ligand-Passivated CsPbI3 Perovskite Nanocrystals for Stable Near-Unity Photoluminescence Quantum Yield and Efficient Red Light-Emitting Diodes. *J. Am. Chem. Soc.* **2018,** *140* (2), 562-565.
28. Kumar, S.; Jagielski, J.; Kallikounis, N.; Kim, Y. H.; Wolf, C.; Jenny, F.; Tian, T.; Hofer, C. J.; Chiu, Y. C.; Stark, W. J.; Lee, T. W.; Shih, C. J., Ultrapure Green Light-Emitting Diodes Using Two-Dimensional Formamidinium Perovskites: Achieving Recommendation 2020 Color Coordinates. *Nano Lett.* **2017,** *17* (9), 5277-5284.
29. Kim, Y.-H.; Cho, H.; Lee, T.-W., Metal halide perovskite light emitters. *Proc. Natl. Acad. Sci. U.S.A* **2016,** *113* (42), 11694-11702.
30. Gangishetty, M. K.; Hou, S.; Quan, Q.; Congreve, D. N., Reducing Architecture Limitations for Efficient Blue Perovskite Light-Emitting Diodes. *Adv. Mater.* **2018,** *30* (20), 1706226.
31. Yao, E. P.; Yang, Z.; Meng, L.; Sun, P.; Dong, S.; Yang, Y.; Yang, Y., High-Brightness Blue and White LEDs based on Inorganic Perovskite Nanocrystals and their Composites. *Adv. Mater.* **2017,** *29* (23), 1606859.
32. Sadhanala, A.; Ahmad, S.; Zhao, B.; Giesbrecht, N.; Pearce, P. M.; Deschler, F.; Hoye, R. L.; Godel, K. C.; Bein, T.; Docampo, P.; Dutton, S. E.; De Volder, M. F.; Friend, R. H., Blue-Green Color Tunable Solution Processable Organolead Chloride-Bromide

Mixed Halide Perovskites for Optoelectronic Applications. *Nano Lett.* **2015,** *15* (9), 6095-6101.

33. Kumawat, N. K.; Dey, A.; Kumar, A.; Gopinathan, S. P.; Narasimhan, K. L.; Kabra, D., Band Gap Tuning of CH(3)NH(3)Pb(Br(1-x)Clx)(3) Hybrid Perovskite for Blue Electroluminescence. *ACS Appl. Mater. Interfaces* **2015,** *7* (24), 13119-13124.

34. Weidman, M. C.; Seitz, M.; Stranks, S. D.; Tisdale, W. A., Highly Tunable Colloidal Perovskite Nanoplatelets Through Variable Cation, Metal, and Halide Composition. *ACS Nano* **2016,** *10* (8), 7830-7839.

35. Kumar, S.; Jagielski, J.; Yakunin, S.; Rice, P.; Chiu, Y.-C.; Wang, M.; Nedelcu, G.; Kim, Y.; Lin, S.; Santos, E. J.; Kovalenko, M. V.; Shih, C.-J., Efficient blue electroluminescence using quantum-confined two-dimensional perovskites. *ACS Nano* **2016,** *10* (10), 9720-9729.

36. Shamsi, J.; Dang, Z.; Bianchini, P.; Canale, C.; Di Stasio, F.; Brescia, R.; Prato, M.; Manna, L., Colloidal synthesis of quantum confined single crystal CsPbBr3 nanosheets with lateral size control up to the micrometer range. *J. Am. Chem. Soc.* **2016,** *138* (23), 7240-7243.

37. Weidman, M. C.; Goodman, A. J.; Tisdale, W. A., Colloidal halide perovskite nanoplatelets: An exciting new class of semiconductor nanomaterials. *Chem. Mater.* **2017,** *29* (12), 5019-5030.

38. Bohn, B. J.; Tong, Y.; Gramlich, M.; Lai, M. L.; Doblinger, M.; Wang, K.; Hoye, R. L. Z.; Muller-Buschbaum, P.; Stranks, S. D.; Urban, A. S.; Polavarapu, L.; Feldmann, J., Boosting Tunable Blue Luminescence of Halide Perovskite Nanoplatelets through Postsynthetic Surface Trap Repair. *Nano Lett.* **2018,** *18* (8), 5231-5238.

39. Pedesseau, L.; Sapori, D.; Traore, B.; Robles, R.; Fang, H. H.; Loi, M. A.; Tsai, H.; Nie, W.; Blancon, J. C.; Neukirch, A.; Tretiak, S.; Mohite, A. D.; Katan, C.; Even, J.; Kepenekian, M., Advances and Promises of Layered Halide Hybrid Perovskite Semiconductors. *ACS Nano* **2016,** *10* (11), 9776-9786.

40. Vybornyi, O.; Yakunin, S.; Kovalenko, M. V., Polar-solvent-free colloidal synthesis of highly luminescent alkylammonium lead halide perovskite nanocrystals. *Nanoscale* **2016,** *8* (12), 6278-6283.

41. Stoumpos, C. C.; Cao, D. H.; Clark, D. J.; Young, J.; Rondinelli, J. M.; Jang, J. I.; Hupp, J. T.; Kanatzidis, M. G., Ruddlesden−Popper hybrid lead iodide perovskite 2D homologous semiconductors. *Chem. Mater.* **2016,** *28* (8), 2852-2867.

42. Bekenstein, Y.; Koscher, B. A.; Eaton, S. W.; Yang, P.; Alivisatos, A. P., Highly Luminescent Colloidal Nanoplates of Perovskite Cesium Lead Halide and Their Oriented Assemblies. *J. Am. Chem. Soc.* **2015,** *137* (51), 16008-16011.

43. Gong, X.; Voznyy, O.; Jain, A.; Liu, W.; Sabatini, R.; Piontkowski, Z.; Walters, G.; Bappi, G.; Nokhrin, S.; Bushuyev, O.; Yuan, M.; Comin, R.; McCamant, D.; Kelley, S. O.; Sargent, E. H., Electron-phonon interaction in efficient perovskite blue emitters. *Nat. Mater.* **2018,** *17* (6), 550-556.

44. Sichert, J. A.; Tong, Y.; Mutz, N.; Vollmer, M.; Fischer, S.; Milowska, K. Z.; Garcia Cortadella, R.; Nickel, B.; Cardenas-Daw, C.; Stolarczyk, J. K.; Urban, A. S.; Feldmann, J., Quantum Size Effect in Organometal Halide Perovskite Nanoplatelets. *Nano Lett.* **2015,** *15* (10), 6521-6527.

45. Gao, Y.; Weidman, M. C.; Tisdale, W. A., CdSe Nanoplatelet Films with Controlled Orientation of their Transition Dipole Moment. *Nano Lett.* **2017,** *17* (6), 3837-3843.

46. Schuller, J. A.; Karaveli, S.; Schiros, T.; He, K.; Yang, S.; Kymissis, I.; Shan, J.; Zia, R., Orientation of luminescent excitons in layered nanomaterials. *Nat. Nanotech.* **2013,** *8* (4), 271-276.

47. Mitzi, D. B.; Feild, C. A.; Harrison, W. T. A.; Guloy, A. M., Conducting tin halides with a layered organic-based perovskite structure. *Nature* **1994,** *369* (6480), 467-469.

48. Pan, J.; Quan, L. N.; Zhao, Y.; Peng, W.; Murali, B.; Sarmah, S. P.; Yuan, M.; Sinatra, L.; Alyami, N. M.; Liu, J.; Yassitepe, E.; Yang, Z.; Voznyy, O.; Comin, R.; Hedhili, M. N.; Mohammed, O. F.; Lu, Z. H.; Kim, D. H.; Sargent, E. H.; Bakr, O. M., Highly Efficient Perovskite-Quantum-Dot Light-Emitting Diodes by Surface Engineering. *Adv. Mater.* **2016,** *28* (39), 8718-8725.

49. Wang, Q.; Ren, J.; Peng, X.-F.; Ji, X.-X.; Yang, X.-H., Efficient Sky-Blue Perovskite Light-Emitting Devices Based on Ethylammonium Bromide Induced Layered Perovskites. *ACS Appl. Mater. Interfaces* **2017,** *9* (35), 29901-29906.

50. Wu, Y.; Wei, C.; Li, X.; Li, Y.; Qiu, S.; Shen, W.; Cai, B.; Sun, Z.; Yang, D.; Deng, Z.; Zeng, H., In Situ Passivation of PbBr64−Octahedra toward Blue Luminescent CsPbBr3 Nanoplatelets with Near 100% Absolute Quantum Yield. *ACS Energy Lett.* **2018,** *3* (9), 2030-2037.

51. Jagielski, J.; Kumar, S.; Wang, M.; Scullion, D.; Lawrence, R.; Li, Y.-T.; Yakunin, S.; Tian, T.; Kovalenko, M. V.; Chiu, Y.-C.; Santos, E. J. G.; Lin, S.; Shih, C.-J., Aggregation-induced emission in lamellar solids of colloidal perovskite quantum wells. *Sci. Adv.* **2017,** *3* (12), eaaq0208.

52. Congreve, D. N.; Weidman, M. C.; Seitz, M.; Paritmongkol, W.; Dahod, N. S.; Tisdale, W. A., Tunable Light-Emitting Diodes Utilizing Quantum-Confined Layered Perovskite Emitters. *ACS Photonics* **2017,** *4* (3), 476-481.

53. Wang, Y.; Li, X.; Sreejith, S.; Cao, F.; Wang, Z.; Stuparu, M. C.; Zeng, H.; Sun, H., Photon Driven Transformation of Cesium Lead Halide Perovskites from Few-Monolayer Nanoplatelets to Bulk Phase. *Adv. Mater.* **2016,** *28* (48), 10637-10643.

54. deMello, J. C.; Wittmann, H. F.; Friend, R. H., An improved experimental determination of external photoluminescence quantum efficiency. *Advanced Materials* **1997,** *9* (3), 230-&.

55. Zhang, Y.-Y.; Chen, S.; Xu, P.; Xiang, H.; Gong, X.-G.; Walsh, A.; Wei, S.-H., Intrinsic instability of the hybrid halide perovskite semiconductor CH3NH3PbI3. *Chin. Phys. Lett.* **2018,** *35* (3), 036104.

56. Yuan, Y.; Huang, J., Ion Migration in Organometal Trihalide Perovskite and Its Impact on Photovoltaic Efficiency and Stability. *Acc. Chem. Res.* **2016,** *49* (2), 286-293.

57. Huang, S.; Li, Z.; Wang, B.; Zhu, N.; Zhang, C.; Kong, L.; Zhang, Q.; Shan, A.; Li, L., Morphology Evolution and Degradation of CsPbBr3 Nanocrystals under Blue Light-Emitting Diode Illumination. *ACS Appl. Mater. Interfaces* **2017,** *9* (8), 7249-7258.

58. Gonzalez-Carrero, S.; Galian, R. E.; Pérez-Prieto, J., Maximizing the emissive properties of CH 3 NH 3 PbBr 3 perovskite nanoparticles. *J. Mater. Chem. A* **2015,** *3* (17), 9187-9193.

59. Yan, K.; Long, M.; Zhang, T.; Wei, Z.; Chen, H.; Yang, S.; Xu, J., Hybrid halide perovskite solar cell precursors: colloidal chemistry and coordination engineering behind device processing for high efficiency. *J. Am. Chem. Soc.* **2015,** *137* (13), 4460-4468.

60. Boonmongkolras, P.; Kim, D.; Alhabshi, E. M.; Gereige, I.; Shin, B., Understanding effects of precursor solution aging in triple cation lead perovskite. *RSC Adv.* **2018,** *8* (38), 21551-21557.

61. Long, M.; Zhang, T.; Chai, Y.; Ng, C. F.; Mak, T. C.; Xu, J.; Yan, K., Nonstoichiometric acid-base reaction as reliable synthetic route to highly stable CH3NH3PbI3 perovskite film. *Nat. Commun.* **2016,** *7*, 13503.

62. McMeekin, D. P.; Wang, Z.; Rehman, W.; Pulvirenti, F.; Patel, J. B.; Noel, N. K.; Johnston, M. B.; Marder, S. R.; Herz, L. M.; Snaith, H. J., Crystallization Kinetics and Morphology Control of Formamidinium−Cesium Mixed-Cation Lead Mixed-Halide Perovskite via Tunability of the Colloidal Precursor Solution. *Adv. Mater.* **2017,** *29* (29), 1607039.

63. Goldschmidt, V. M., The laws of crystal chemistry. *Naturwissenschaften* **1926,** *14* (21), 477-485.

64. Saparov, B.; Mitzi, D. B., Organic−inorganic perovskites: structural versatility for functional materials design. *Chem. Rev.* **2016,** *116* (7), 4558-4596.

65. Jeon, N. J.; Noh, J. H.; Yang, W. S.; Kim, Y. C.; Ryu, S.; Seo, J.; Seok, S. I., Compositional engineering of perovskite materials for high-performance solar cells. *Nature* **2015,** *517* (7535), 476-480.

66. Saidaminov, M. I.; Kim, J.; Jain, A.; Quintero-Bermudez, R.; Tan, H.; Long, G.; Tan, F.; Johnston, A.; Zhao, Y.; Voznyy, O.; Sargent, E. H., Suppression of atomic vacancies via incorporation of isovalent small ions to increase the stability of halide perovskite solar cells in ambient air. *Nat. Energy* **2018,** *3* (8), 648-654.

67. Li, Z.; Yang, M.; Park, J.-S.; Wei, S.-H.; Berry, J. J.; Zhu, K., Stabilizing perovskite structures by tuning tolerance factor: formation of formamidinium and cesium lead iodide solid-state alloys. *Chem. Mater.* **2015,** *28* (1), 284-292.

68. Kieslich, G.; Sun, S.; Cheetham, A. K., Solid-state principles applied to organic–inorganic perovskites: new tricks for an old dog. *Chem. Sci.* **2014,** *5* (12), 4712-4715.

69. Dou, L. T.; Wong, A. B.; Yu, Y.; Lai, M. L.; Kornienko, N.; Eaton, S. W.; Fu, A.; Bischak, C. G.; Ma, J.; Ding, T. N.; Ginsberg, N. S.; Wang, L. W.; Alivisatos, A. P.; Yang, P. D., Atomically thin two-dimensional organic-inorganic hybrid perovskites. *Science* **2015,** *349* (6255), 1518-1521.

70. Merdasa, A.; Bag, M.; Tian, Y.; Källman, E.; Dobrovolsky, A.; Scheblykin, I. G., Super-Resolution Luminescence Microspectroscopy Reveals the Mechanism of Photoinduced Degradation in CH3NH3PbI3Perovskite Nanocrystals. *J. Phys. Chem. C* **2016,** *120* (19), 10711-10719.

71. Tan, H.; Che, F.; Wei, M.; Zhao, Y.; Saidaminov, M. I.; Todorović, P.; Broberg, D.; Walters, G.; Tan, F.; Zhuang, T.; Sun, B.; Liang, Z.; Yuan, H.; Fron, E.; Kim, J.; Yang, Z.; Voznyy, O.; Asta, M.; Sargent, E. H., Dipolar cations confer defect tolerance in wide-bandgap metal halide perovskites. *Nat. Commun.* **2018,** *9*, 3100.

72. Kirchnerová, J.; Cave, G. C. B., The solubility of water in low-dielectric solvents. *Can. J. Chem.* **1976,** *54* (24), 3909-3916.

73. Gottesman, R.; Haltzi, E.; Gouda, L.; Tirosh, S.; Bouhadana, Y.; Zaban, A.; Mosconi, E.; De Angelis, F., Extremely Slow Photoconductivity Response of CH3NH3PbI3 Perovskites Suggesting Structural Changes under Working Conditions. *J. Phys. Chem. Lett.* **2014,** *5* (15), 2662-2669.

74. Manser, J. S.; Saidaminov, M. I.; Christians, J. A.; Bakr, O. M.; Kamat, P. V., Making and Breaking of Lead Halide Perovskites. *Acc. Chem. Res.* **2016,** *49* (2), 330-338.

75. De Roo, J.; Ibanez, M.; Geiregat, P.; Nedelcu, G.; Walravens, W.; Maes, J.; Martins, J. C.; Van Driessche, I.; Kovalenko, M. V.; Hens, Z., Highly Dynamic Ligand Binding and Light Absorption Coefficient of Cesium Lead Bromide Perovskite Nanocrystals. *ACS Nano* **2016,** *10* (2), 2071-2081.

76. Azpiroz, J. M.; Mosconi, E.; Bisquert, J.; De Angelis, F., Defect migration in methylammonium lead iodide and its role in perovskite solar cell operation. *Energy Environ. Sci.* **2015,** *8* (7), 2118-2127.
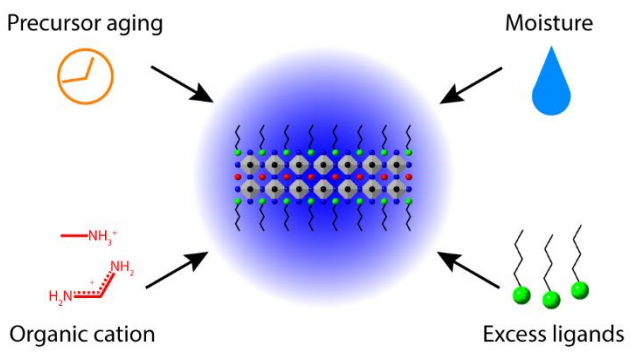
Table of Contents artwork